JOURNAL OF SOLID STATE CHEMISTRY 59, 242–249 (1985)

A Neutron Diffraction and ^{170}Yb Mössbauer Investigation of the Perovskite Ytterbium Titanium Oxide

J. E. GREEDAN

Institute for Materials Research and Department of Chemistry, Mc Master University, Hamilton L8S 4M1, Canada

AND LYNNE SODERHOLM AND J. M. FRIEDT

Centre de Recherches Nucleaires, B. P. 20-67037 Strasbourg Cedex, France

Received October 17, 1984; in revised form February 28, 1985

A phase with the perovskite structure (*Pbnm*) and a composition $YbTiO_{2.95}$ has been prepared by a high-temperature carbothermic method. Neutron diffraction shows a colinear ferrimagnetic structure at 7 K with Yb and Ti moments antiparallel along the *c*-axis of the orthorhombic cell and an Yb moment of $1.8(3)\mu_B$. ^{170}Yb Mössbauer measurements find a more precise and accurate value of $2.0(1)\mu_B$ from the maximum hyperfine field. From the temperature dependence of the hyperfine field a $T_c = 42(1)$ K is found. The Yb sublattice magnetization below T_c follows a Brillouin function. At low temperature a distribution of hyperfine fields is observed which is attributed to a random distribution of defects surrounding the Yb sites. The magnetic structure is discussed in relation to possible values for the crystal field parameters, especially B_0^2.

Introduction

There has been considerable progress made recently toward the characterization of the magnetic properties of the series $RTiO_3$ (R = Gd → Tm, Y) (*1–6*). These compounds crystallize in an orthorhombic distortion of the cubic perovskite structure, and are isostructural with the $GdFeO_3$ family AMO_3 (A = rare earth; M = Al, Ga, V, Cr, Mn, Co, Fe) (*7*). The titanates are unique among this family because the Ti(+3) atoms, with 1*d* electron, order ferromagnetically, producing an appreciable exchange field at R. Expressed as an effective field, the R–Ti interaction produces about 10^5 Oe at R, compared to 10^3–10^4 Oe for R–Fe and R–Cr (*4*). Furthermore, the R–Ti exchange interaction is largely isotropic symmetric rather than antisymmetric as in R–Cr and R–Fe (*4*). Despite these differences, common features have emerged (*4*) between the magnetic structures of the RMO_3 phases.

The site symmetry at $R(C_s)$ limits the easy direction to be either in the a–b (mirror) plane, or along the c-axis. For the known structures of $TbMO_3$, $DyMO_3$, and $HoMO_3$ (M = Al, Fe, Cr, Co, Ti), the R moment always lies in the a–b plane, while for $ErMO_3$ and $TmMO_3$ it is always parallel to the c-axis.

This behavior likely corresponds to the rare-earth single-ion anisotropy dominating the R–M coupling. A simple model was used to calculate the anisotropy for the $RTiO_3$ series (*4*). Briefly, this consists of the diagonalization within the basis of the

0022-4596/85 $3.00

R^{3+} free-ion wavefunction of the R-site Hamiltonian $\mathcal{H}_R = \mathcal{H}_{CF} + \mathcal{H}_{mol.}$. Here, $\mathcal{H}_{CF}$ is the crystal field at R expressed in the Racah formalism as a sum over terms $B_q^k C_q^k$ (*8*). $\mathcal{H}_{mol.}$ is the effective exchange field at R due to the Ti sublattice and is equal to $g_J \mu_B \tilde{J}_z H_{mol.}$ for the field component along c or $g_J \mu_B \tilde{J}_x H_{mol.}$ for the field component normal to c (a–b plane).

Values for the B_q^k's were taken as determined by O'Hare and Donlan for Er^{3+} in $YAlO_3$ (*9*). When R = Tb, Dy, or Ho the configuration with the R moment $\perp_c$ is more stable and when R = Er or Tm the R moment is found $\|_c$.

These results correlate well with the sign of the matrix element $\langle SLJM_J|B_0^2C_0^2|SLJM_J\rangle$. For R = Tb, Dy, or Ho this term is > 0 for R = Er or Tm it is < 0. For R = Yb the matrix element is also < 0 and c-axis anisotropy is anticipated, qualitatively.

Quantitatively, the results of similar calculations for $YbTiO_3$ are far more ambiguous than for the other heavy rare-earth $RTiO_3$ phases. In Table I we give results of four different calculations using various sets of published CF parameters for the R site in $YAlO_3$, denoted as A, B, C, and D. A is the set used previously, C_s symmetry, $Er^{3+}:YAlO_3$ (*9*). B is for $Tm^{3+}:YAlO_3$ (*10*). Set C, previously unavailable, is for $Yb^{3+}:YAlO_3$ (*11*) and D is also for $Tm^{3+}:YAlO_3$ but in the D_{4h} approximation which features a much larger B_0^2 term than the other models (*10*).

TABLE I

RESULTS FOR Yb^{3+} ANISOTROPY AT THE R-SITE FOR DIFFERENT SETS OF CRYSTAL FIELD PARAMETERS

CF model (B_0^2 in K)	E_0(K) $\mathcal{H}CF+\mathcal{H}mol\|c$	E_0(K) $\mathcal{H}CF+\mathcal{H}mol\perp c$	Predicted moment direction	Calculated Yb moment μ_B
A (−265.1)	−314.0	−314.8	?	0.60
B (−630.3)	−449.2	−445.3	?	0.76
C (−260.8)	−384.0	−388.8	$\perp_c$	2.1
D (−1241.4)	−418.6	−404.7	$\|_c$	2.1

Models A and B give no clear prediction of the Yb moment direction while models C and D predict opposite results. Both C and D give an Yb^{3+} moment of $2.1\mu_B$.

Experimental results on other $YbMO_3$ phases are equally ambiguous regarding predictions for $YbTiO_3$. The Yb moment in $YbFeO_3$ (above the reorientation temperature, T_R) is along c with a moment of $0.3\ \mu_B$ at 10 K (*12*) much quenched from the free-ion value of $4.0\ \mu_B$. In $YbCrO_3$ there is no order on the Yb sublattice down to 1.3 K [*13*]. $YbAlO_3$ orders magnetically at 0.8 K (*14, 15*) with an Yb moment at $2.49\ \mu_B$ in the a–b plane.

Little is known about the penultimate member of the $RTiO_3$ series, $YbTiO_3$. It has not been synthesized as a pure phase, but powder samples containing about 10% of a paramagnetic impurity have been prepared. Magnetic measurements show that the perovskite phase orders at 39(2) K but no saturation effects are seen at 4.2 K up to 5.0 T (*3*). As neither the direction nor the magnitude of the Yb moment in $YbTiO_3$ can be determined from such powder magnetic data, this material has been investigated using the complementary techniques of neutron diffraction and ^{170}Yb Mössbauer spectroscopy.

Experimental

Sample preparation and characterization. Techniques which can be used for the preparation of other $RTiO_3$ phases give poor results for $YbTiO_3$. Both arc melting of Yb_2O_3 and Ti_2O_3 under an argon atmosphere and the firing of mixtures of these same starting materials in welded Mo crucibles yield products consisting of a perovskite and relatively large amounts (>30%) of a second phase which is identified as the pyrochlore $Yb_2Ti_2O_7$ (*16*). Better results can be obtained using a carbothermic technique as shown below (*17*):

$$Yb_2O_3 + 2TiO_2 + C \xrightarrow[\substack{10^{-5}\ \text{Torr}\\ 2\rightarrow 3\ \text{hr}}]{1600^\circ C} 2YbTiO_3 + CO$$

This procedure yields a perovskite with cell constants $a = 5.256$ Å, $b = 5.662$ Å, and $c = 7.540$ Å and only 10% of the pyrochlore. The cell volume of the perovskite, 224.4 (Å)^3, lies between that of $TmTiO_3$, 226.8 (Å)^3, and $LuTiO_3$, 220.0 (Å)^3.

Thermal gravimetric analysis, performed on the perovskite/10% pyrochlore mixture, reveals a 3.05(5)% weight gain, consistent with that of a pure perovskite $YbTiO_3$ (2.97%), but larger than that expected (2.64%) for a mixture with a fully oxidized pyrochlore. This result can be explained by assuming the incorporation of oxygen vacancies into the perovskite phase. That is, the mixture corresponds to 0.90 $YbTiO_{2.95}$ + 0.10 $YbTiO_{3.50}$.

Neutron diffraction. Data were obtained at the McMaster Nuclear Reactor on a triple-axis spectrometer operating in the double-axis mode with a wavelength of 1.40 Å and a position-sensitive detector. This system has been described elsewhere (*18*). Temperature control was provided by a CTI Inc. Model 21 closed-cycle refrigerator and a Cryogenics Inc. Model DRC 80C controller. Temperatures were measured with a germanium resistance thermometer and control was in all cases better than ±0.5 K. Samples were contained in a thin-walled aluminum cell filled with helium exchange gas and sealed with an indium gasket.

Mössbauer effect. ^{170}Yb Mössbauer spectra, involving the 84.4-keV E2 transition between spin states $0^+ \rightarrow 2^+$ were measured in the transmission geometry using a powdered absorber. The source of TmB_{12}, providing an experimental minimum resonance width of 2.7 mm sec^{-1} was maintained at 4.2 K while the sample temperature was held constant between 4.2 and 50 K.

Results

Neutron Diffraction

The direction of the R^{3+} moment in the $RTiO_3$ perovskites can be determined directly from the gross features of the magnetic powder pattern. The detailed arguments have been given previously but a brief summary follows (*3*, *4*). The R^{3+} lies on a mirror plane normal to the *c*-axis. Therefore, one of the principal axes of the anisotropy or *g*-tensor must lie parallel to the *c*-axis and the other two in the *a*–*b* plane. Of the axes in the plane, symmetry does not require any special relation to the *a* or *b* directions and in all known cases these axes lie at some angle to *a* or *b*. If the moment lies in the *a*–*b* plane the symmetry operations of *Pbnm* require the coexistence of both ferromagnetic, *F*, and antiferromagnetic components, *C*. If the moment lies parallel to *c* either F_z or C_z configurations are allowed but in the $RTiO_3$ compounds only F_z has been observed.

The chemical or nuclear cell in the $RTiO_3$ phase has the space group *Pbnm* so reflections of the type (0*kl*), $k = 2n + 1$ and (*h*0*l*), $h + l = 2n + 1$ are systematically absent. If the *R* sublattice has configuration *F* there are no new magnetic reflections and enhanced intensities are expected for reflections of the type $h + k = 2n$, $l = 2n$. There will also be weak enhancements of the $h + k = 2n$, $l = 2n + 1$ reflections (*A* type) because the R^{3+} ions are only slightly displaced from special positions in the chemical cell. If the *R* sublattice moment has a *C* component, new reflections of the type $h + k = 2n + 1$, $l = 2n$ will appear which in some cases violate the *Pbnm* symmetry rules, for example, (100), (010), (012), and (102).

To summarize, if the *R* moment lies in the *ab* plane new reflections of the *C* type appear in the magnetic powder pattern. If the *R* moment lies along *c*, only *F*-type reflections will be seen.

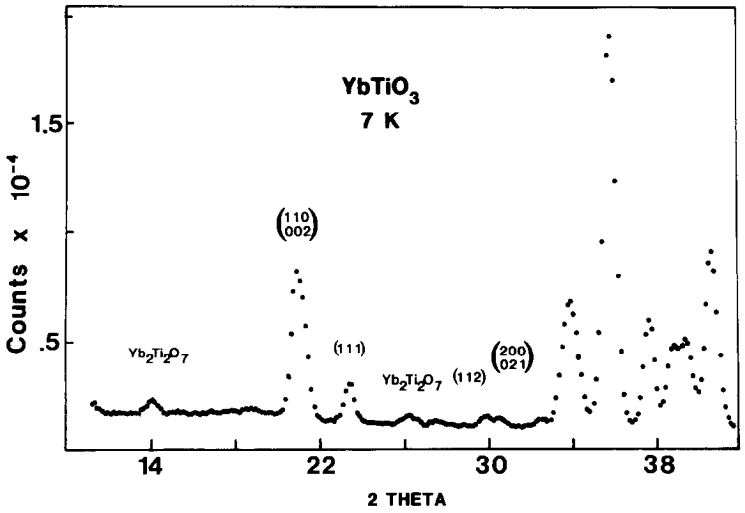

FIG. 1. The neutron diffraction pattern at 7 K of the mixture 90% $YbTiO_{2.95}$/10% $Yb_2Ti_2O_7$.

Neutron diffraction powder patterns for $YbTiO_3$, $T_c = 41$ K, were obtained at 7 and 50 K. The pattern at 7 K is shown in Fig. 1. All lines can be indexed on the *Pbnm* cell except for two lines of 2θ values 14.0 and 26.4 which are assigned to the (111) and (222,311) reflections of the pyrochlore, $Yb_2Ti_2O_7$. The absence of new Bragg peaks in the 7 K pattern gives immediate indication that the Yb moment is ferromagnetic along the c direction.

By comparing the integrated intensities of the low-angle reflections significant enhancement is observed for only three groups of intensities (110, 002), (111), and (112, 200, 021). This is shown in Fig. 2 and in Table II.

As the reflections (112) and (200,021) are

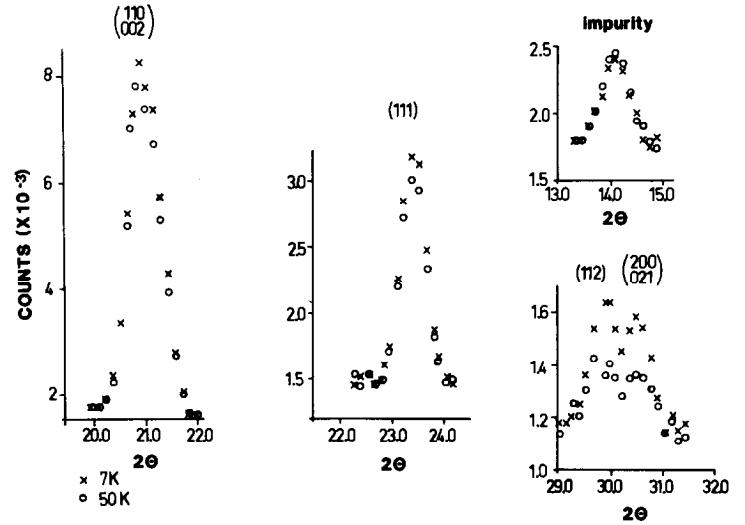

FIG. 2. A comparison of diffracted intensities at 7 and 50 K for low-angle reflections of $YbTiO_{2.95}$.

TABLE II

OBSERVED AND CALCULATED MAGNETIC INTENSITIES FOR $YbTiO_3$

hkl	I_{obs}^{mag} ($I_{7\,K}-I_{50\,K}$)	I_{mag}^{calc} (Ti = $-0.8\mu_B$, Yb = $1.7\mu_B$)	I_{mag}^{calc} (Ti = $-0.5\mu_B$, Yb = $1.9\mu_B$)
(110,002)	392 (49)	408	376
(111)	73 (22)	74	85
(112)	82 (23)	30	68
(200,021)	86 (23)	90	124
		$R = 0.09$	$R = 0.13$

clearly resolved the intensities were determined separately by fitting this region of the pattern to two Gaussians with a linear background using a standard nonlinear squares technique.

As there are three parameters (a scale factor and two magnetic moments) and only four observed intensities, a true refinement is not possible. Instead, intensities were calculated for a number of models in which the Yb moment and the Ti moment magnitudes were varied systematically.

Previous refinements of other $RTiO_3$ structures reveal that the Ti moment varies between 0.5 and 0.8 μ_B (*2*). Therefore, the Ti moment was fixed along z antiparallel to the Yb moment, and the Yb moment varied for both extreme values of the Ti moment. Those models giving the best agreement with I_{obs} are also shown in Table I. Note that the two values for the Yb moment differ by slightly more than 10% and that their mean value is 1.8 B.M.

Mössbauer Spectroscopy

^{170}Yb Mössbauer spectra of the mixture are shown for selected temperatures in Fig. 3. The spectra at 43 and 50 K reveal a static paramagnetic spectrum split by the presence of a nonaxial electric field gradient (EFG), with independent components $e^2qQ = 20.9(6)$ mm sec^{-1} and an asymmetry parameter $\eta = 0.4$.

Below 40 K, down to 4.2 K, a further splitting is observed, revealing the presence of a magnetic hyperfine field at the Yb site. Electric quadrupole and magnetic dipole interactions of comparable magnitude necessitate the simultaneous diagonalization of the nuclear hyperfine Hamiltonian for noncoaxial magnetic and quadrupolar hyperfine interactions for these low-temperature spectra. An unresolved quadrupole pattern, corresponding to the presence of 10% of the pyrochlore phase (*19*), is included in all the data analyses.

The temperature dependence of the Mössbauer spectra reveals a magnetic ordering temperature of 42(1) K, in good agreement with the value of 39(1) K established from magnetization measurements. However, the temperature-dependent line broadening observed below 40 K requires an interpretation either in terms of magnetic relaxation, or in terms of a distribution of the hyperfine parameters. Although technically feasible, a model of relaxation between the substates of the ground Kramers doublet, split by the exchange field (*20*), provides physically unreasonable results. The relaxation rate strongly de-

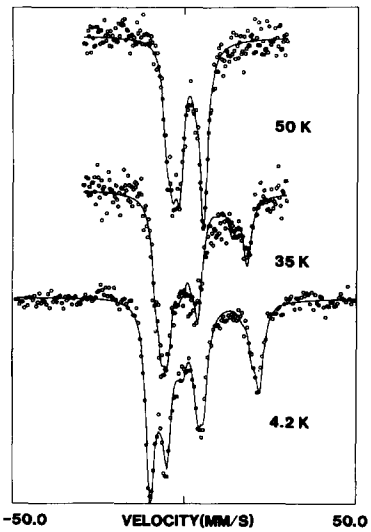

FIG. 3. $YbTiO_{2.95}$: ^{170}Yb Mössbauer spectra at various temperatures.

creases on lowering the temperature, whereas a spin–lattice coupling mechanism, which would operate in the considered temperature range, predicts nearly temperature-independent behavior (*21*).

The low-temperature (<40 K) data were instead interpreted in terms of a static distribution of the hyperfine field parameters. This situation is assigned to a distribution of superexchange interactions resulting from defects incorporated into the sample. That is, magnetic order on the Yb sublattice is induced by coupling to the Ti sublattice through Yb–O–Ti linkages. The proposed stoichiometry of the perovskite phase is $YbTiO_{2.95}$ which can also be written as $Yb^{III}Ti^{III}_{0.90}Ti^{II}_{0.10}O_{2.95}\square_{0.05}$ with defects on both the oxygen and titanium sublattices. For this model the total concentration of defects surrounding a single Yb atom is 6%, assuming a random distribution among the nearest neighbor oxygen and titanium atoms (eight of each).

The analysis is performed using a histogram method for the distribution of the hyperfine field. The relative intensities of the three histogram components are obtained assuming a statistical (binomial) distribution of the 6% of defects among the Yb nearest neighbors. The component linewidth is maintained at the experimental value (2.7 mm sec^{-1}); the EFG principal component, the maximum hyperfine field, the difference in hyperfine field between the histogram components (Δ), and the total absorption are adjustable parameters. The results are shown in Table III.

The Yb(+3) moment magnitude scales with the hyperfine field (1050 kOe/μ_B) (*22*), hence the moment is directly determined from the maximum hyperfine field component of the spectrum (zero nearest-neighbor vacancies). It is found to be 2.0(1) μ_B at 4.2 K and has a temperature dependence which is well represented by a Brillouin function, as shown in Fig. 4.

The evaluation of the magnetic structure

TABLE III

^{170}Yb MÖSSBAUER PARAMETERS AS A FUNCTION OF TEMPERATURE FOR $YbTiO_3$

Temp. (°K)	e^2qQ (mm/sec)	HM (kOe)	Δ (kOe)
4.2	24 (1)	2120 (100)	400 (50)
20	24 (1)	2020 (100)	300 (50)
30	21 (1)	1800 (100)	700 (50)
35	21 (1)	1650 (100)	600 (50)
40	23 (1)	1290 (100)	700 (50)
50	21 (1)	—	—

Note. ^{170}Yb Mössbauer parameters obtained assuming a distribution of hyperfine fields. HM is the maximum field with H at the other histogram site determined from $H = HM - n\Delta$ where n is the number of *nn* vacancies. $\eta = 0.38$ was determined from the 50 K data and fixed for $T < 50$ K. Errors are in parentheses.

of the perovskite phase from the Mössbauer data can be discussed in terms of the relative orientation between the hyperfine field, H_z (i.e., magnetic moment) and the principal axis of the EFG. Although the *RE* site symmetry (C_s) dictates that the EFG and magnetic hyperfine field tensors must have one axis along the crystallographic c direction, there is no a priori requirement that either V_{zz}, the EFG component along the EFG principal axis, or H_z be along c, nor that they be parallel. The angle between V_{zz} and H_z must be determined from the data. Knowing the field gradient parameters from the paramagnetic state, which do not change significantly with decreasing temperature, it is found that the low-temperature spectra are only consistent with a coincident axis system for the two tensors, i.e., V_{zz} and H_Z are parallel. As the direction of H_z is known from the neutron diffraction results to be parallel to c, V_{zz} is also parallel to c.

In general the EFG tensor is composed of two parts: EFG $= eQV_{zz}^{latt}(1 - \gamma_\infty) + eQV_{zz}^{latt}(1 - R)$ where V_{zz}^{latt} and V_{zz}^{val} represent the lattice and unpaired $4f$ electron contributions and $(1 - \gamma_\infty)$ and $(1 - R)$ are shielding parameters (*24*). Lattice sum calculations

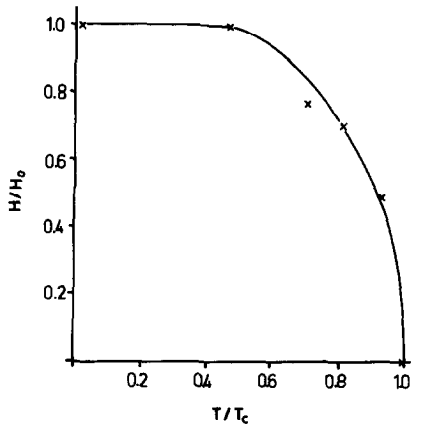

FIG. 4. $YbTiO_{2.95}$: temperature dependence of the average ^{170}Yb hyperfine field.

place V_{zz}^{latt} normal to c about 30° from the a-axis [23]. That V_{zz} for the total EFG tensor lies parallel to the c-axis indicates the not-surprising dominance of the $4f$ contribution. In principle it is possible to calculate the $4f$ contribution from a knowledge of the ground state wavefunction but such detailed information is not available.

Discussion and Conclusions

A perovskite material with a composition near $YbTiO_{2.95}$ has been prepared and characterized. Neutron diffraction reveals a colinear ferrimagnetic structure with a Yb moment of 1.8(3) μ_B parallel to the c-axis. A rather large error is associated with the Yb moment obtained by this method. A more precise and accurate value of 2.0(1) μ_B is determined from the magnetic hyperfine field at ^{170}Yb using the Mössbauer effect. The preferred c-axis direction for the Yb moment in $YbTiO_3$ is in accord with qualitative arguments based on the sign of the crystal field (CF) matrix element $<SLJM_J|B_0^2C_0^2|SLJM_J>$. The contents of Table I show that for Yb, quantitative results are very sensitive to the exact values of the *CF* parameters. Of the four sets of existing parameters only set D correctly predicts the moment direction and magnitude. Set D features an unusually large value for the B_0^2 parameter but the D_{4h} symmetry only approximates the true C_s environment.

The Mössbauer spectra showed evidence for a distribution of hyperfine fields at the Yb site. This is understood in terms of the proposed stoichiometry of the perovskite phase, $YbTiO_{2.95}$, and a random distribution of defects.

Acknowledgments

We thank Mr. J. Couper for assistance with the neutron diffraction experiments and Mr. H. F. Gibbs for the thermal gravimetry analysis. We also thank Dr. P. Imbert for obtaining some of the ^{170}Yb Mössbauer data, at CEN, Saclay. Financial support from the National Science and Engineering Research Council of Canada is acknowledged. One of the authors (L. S.) wishes to thank NSERC (Canada) and NATO for financial support.

References

1. C. W. TURNER AND J. E. GREEDAN, *J. Solid State Chem.* **34,** 207 (1980).
2. C. W. TURNER, M. F. COLLINS, AND J. E. GREEDAN, *J. Magn. Magn. Mater.* **20,** 165 (1980).
3. C. W. TURNER, M. F. COLLINS, AND J. E. GREEDAN, *J. Magn. Magn. Mater.* **23,** 265 (1981).
4. C. W. TURNER, AND J. E. GREEDAN, *J. Magn. Magn. Mater.* **36,** 242 (1983).
5. V. G. ZUBKOV, I. F. BERGER, G. V. BAZUEV, AND A. M. ARTAMONOVA, *Sov. Phys. Solid State* **24,** 663 (1982).
6. J. E. GREEDAN, C. W. TURNER, AND D. A. GOODINGS, *J. Magn. Magn. Mater.* **42,** 255 (1984).
7. D. A. MACLEAN, H.-N. NG, AND J. E. GREEDAN, *J. Solid State Chem.* **30,** 35 (1979).
8. B. G. WYBOURNE, "Spectroscopic Properties of Rare Earths," Interscience, New York (1965).
9. J. M. O'HARE AND V. L. DONLAN, *Phys. Rev. B* **15,** 10 (1977).
10. J. M. O'HARE AND V. L. DONLAN, *Phys. Rev. B* **14,** 3732 (1976).
11. K. K. DEB, *J. Phys. Chem. Solids* **43,** 819 (1982).
12. G. R. DAVIDSON, B. D. DUNLAP, M. EIBSCHUTZ, AND L. G. VAN UITERT, *Phys. Rev. B* **12,** 1681 (1975).
13. P. BONVILLE, F. GONZALES-JIMENEZ, P. IMBERT,

AND F. VARRET, *J. Phys. (Paris) Colloq.* **35,** 575 (1974).
14. P. BONVILLE, J. A. HODGES, P. IMBERT, AND F. HARTMANN-BOUTRON, *Phys. Rev. B* **18,** 2196 (1978).
15. P. RADHAKRISHNA, J. HAMMANN, M. OCIO, P. PARI, AND Y. ALLAIN, *Solid State Commun.* **37,** 813 (1981).
16. G. JEHANNO (CEN SACLAY), private communication.
17. G. V. BAZUEV AND G. P. SHVEIKEN, *Russ. J. Inorg. Chem.* **22,** 675 (1977).
18. I. J. DAVIDSON AND J. E. GREEDAN, *J. Solid State Chem.* **51,** 104 (1984).
19. B. D. DUNLAP, G. K. SHENOY, J. M. FRIEDT, M. MEYER, AND G. J. MC CARTHY, *Phys. Rev. B* **18,** 1936 (1978).
20. I. NOWIK AND H. H. WICKMAN, *Phys. Rev. Lett.* **17,** 949 (1966).
21. P. BONVILLE, *Rev. Phys. Appl.* **18,** 365 (1983); P. IMBERT, *Rev. Phys. Appl.* **18,** 457 (1983).
22. C. MEYER, Y. GROS, F. HARTMANN-BOUTRON, AND J. J. CAPPONI, *J. Phys. (Paris)* **40,** 403 (1979).
23. L. SODERHOLM AND C. V. STAGER, unpublished.
24. S. OFER, I. NOWIK, AND S. G. COHEN, *in* "Chemical Applications of Mössbauer Spectroscopy" (V. T. Goldanskii and R. H. Herber, Eds.), pp. 428–503, Academic Press, New York (1968).